A computational study of heat transfer in a laminar oscillating confined slot jet impinging on an isothermal surface at low Reynolds numbers

Johnny ISSA*,[1], Bchara SIDNAWI[1], Najib SALIBA[2]

*Corresponding author
[1]Department of Mechanical Engineering, University of Balamand,
El koura, North Lebanon
johnny.issa@balamand.edu.lb*, bchara_sidnawi@hotmail.com
[2]Department of Civil Engineering, University of Balamand, El koura, North Lebanon
najib.saliba@balamand.edu.lb

DOI: 10.13111/2066-8201.2015.7.3.9

Received: 19 June 2015 / Accepted: 03 July 2015

Abstract: *Heat transfer in a laminar confined oscillating slot jet is numerically investigated. A uniform inlet velocity profile oscillating with an angle φ, having the following sinusoidal shape: $\varphi = \varphi_{max} * \sin(2\pi ft)$. φ is in radians, φ_{max} is the maximum jet angle, and f is the oscillation frequency. The height-to-jet-width ratio (H/w) was fixed to 5 and the fluid's Prandtl number which is one of the dimensionless governing groups is 0.74. The other dimensionless groups characterizing this problem, which are, Strouhal's number, St, and Reynolds number, Re, where varied. Re was in the range $100<Re<400$, and St was in the range $0.05<St<0.75$. Both St and Re numbers are based on the jet hydraulic diameter (2w). Defining φ_{max} is explained later in this paper. For Re=250 and St=0.5, a dim heat transfer enhancement was noticed in the stagnation region, when compared to the steady case. A similar enhancement was observed for Re=400 at St=0.75. At Re=100 no improvements were observed, where the flow showed a high vulnerability to severe oscillations, that drastically reduced heat removal ability. Jet flapping could be triggered at Re=400. But the flapping mode was most stable for St=0.75, in which case, heat transfer enhancement was detected.*

Key Words: *heat transfer, oscillating jet, flapping, Reynolds numbers.*

1. INTRODUCTION

Fluid jets turned out to be very useful in many industrial applications, such as cooling of a heated surface, drying, flow separation control and aerodynamic control. Speaking of cooling, electronic circuits are getting smaller and faster, increasing the density of heat dissipation and giving rise to the necessity of new cooling technologies. Impinging jets are a very promising technology that could catch up with the advancements of the electronics industry. Many numerical and experimental studies were conducted in order to understand the flow fields resulting from fluid jets, and subsequently the heat transfer. In the numerical study of [1], it was shown that a sinusoidal synthetic circular jet, impinging on a heated surface can enhance the overall averaged heat transfer compared to the steady jets that had a higher stagnation Nusselt Number. [2] numerically investigated, two-dimensional, laminar

free and wall pulsed plane jets, where the flow out of the jet had a sinusoidal pulsation. For the wall jet, both adiabatic and isothermal walls were considered. The pulsation could enhance heat transfer by up to 9%. In a numerical study on semi-confined axi-symmetric laminar pulsed impinging water jets [3], it was found that the radial position of flow separation in the wall jet region was the location where the Nusselt number remained constant during one oscillation cycle. This was explained by the existence of vortices above that location, which hinders the acceleration and deceleration of the flow during every oscillation. A numerical investigation of heat transfer in a laminar pulsed slot jet impinging on a surface for low Reynolds numbers [4] showed an improvement of 23% over the continuous case. [5] numerically studied the jet stability problem where the jet had a fixed height-to-width ratio of 5. It was shown that at a Reynolds number between 585 and 610, the jet transitions to a flapping mode, which leads to a heat transfer enhancement when compared to a hypothetical steady jet, when Reynolds number was set to 750. In a detailed experimental study performed by [6], on self-oscillating impinging jets for high Re numbers, the heat transfer coefficient enhancement due to flapping, ranged from 20% to 70% over the stationary jets. In the present study, the heat transfer performance of a sinusoidal self-oscillating impinging jet at H/w=5 (with w=0.01m), but for Reynolds numbers *Re* belonging to the self-stable range presented by the study of Chiriac et al. [5], is numerically investigated. The motivation behind this study, was the heat transfer enhancement found by the numerical study of [5], which was due to flapping. Therefore, it was worthwhile, to try forcing the jet into flapping by virtue of the oscillating inlet conditions, in order to investigate the response of heat transfer; and see if it would exhibit any enhancement.

2. PROBLEM DESCRIPTION

A brief description of the treated problem is illustrated in the figure below.

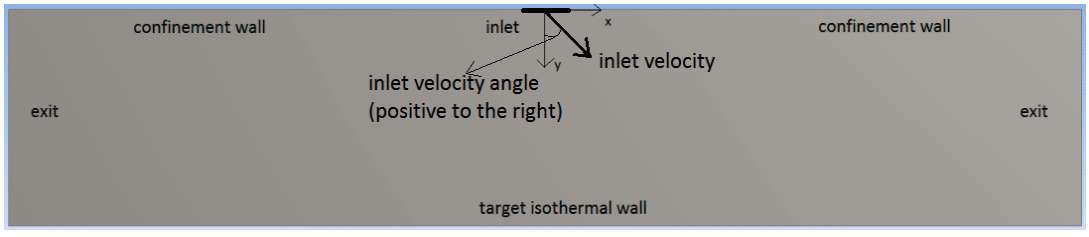

Fig. 1 – A sketch describing the current problem

The working fluid is air having the following properties that are assumed to be constant:

ρ=1.1184 Kg/m^3, C_p=1006.43 J/Kg.K, k=0.0242 W/m.K, μ=1.7894*10^{-5} Kg/m.s

The flow in the channel is unsteady, and assumed to be laminar, incompressible, and two-dimensional. Kinetic dissipation terms in the energy equation are neglected. Hence, the equations to be solved are:

$$\nabla.\vec{V} = 0 \tag{1}$$

$$\frac{D\vec{V}}{Dt} = -\frac{\nabla P}{\rho} + \nu\nabla^2\vec{V} \tag{2}$$

$$\frac{DT}{Dt} = \alpha\nabla^2 T \tag{3}$$

Where $\vec{V}$ is the velocity vector, P is the pressure, ν is the kinematic viscosity, T is the temperature, and α is the thermal diffusivity. The upper wall is adiabatic, and the target wall is isothermal, with assumed no-slip and impermeable conditions for both walls. The set of boundary, and initial conditions, for which the above equations were solved, is:

- At the confinement wall (-12.5w<*x*<-0.5w and 0.5w<*x*<12.5w, *y*=0):

$u = v = 0$ (u and v are the *x* and *y* velocity components, respectively)

$$\frac{\partial T}{\partial y} = 0$$

- At the target wall (-12.5w<*x*<12.5w, *y*/w=H/w=5):

$$u = v = 0$$

$$T = T_w = 310$$

- A zero gradient for all quantities at the exits (*x*/w=-12.5, and *x*/w=12.5):

$$\frac{\partial u}{\partial x} = \frac{\partial v}{\partial x} = \frac{\partial T}{\partial x} = 0$$

- An oscillating, velocity profile at the inlet (-0.5w<*x*<0.5w, *y*=0):

$$V_{inlet} = constant$$

$$\varphi = \varphi_{max} * \sin(2\pi f t)$$

$$T = T_0 = 300 \text{ K}$$

This means, at the inlet:

$$u = V_{inlet} \sin(\varphi)$$

$$v = V_{inlet} \cos(\varphi)$$

- The flow was initiated at *t*=0 as follows:

$$T = T_0 = 300 \text{ K}, \; u = v = 0, \text{ everywhere}$$

φ_{max} was defined based on the location where the space averaged value of the wall Nusselt number distribution, *Nu* occurred, for the steady case of each *Re* considered.

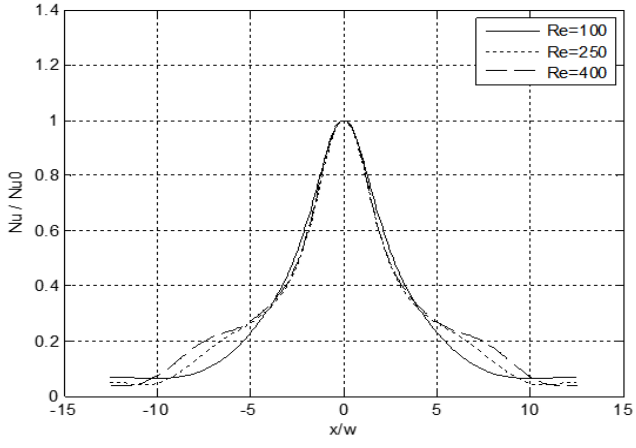

Fig. 2 – The dimensionless Nu distribution for the three corresponding steady cases

As one can see in Fig. 2, each of the three distributions has two symmetric locations, where it starts flattening. Each distribution was averaged between those two symmetric locations.

Then the two span-wise locations ($\pm x_0/w$) where the average value occurred, were taken. The results came as follows:

$$Re=100,\ x_0/w = 3.3.$$

$$Re=250,\ x_0/w = 3.9.$$

$$Re=400,\ x_0/w = 3.8.$$

The average of the three values of x_0/w is 3.67, from which the value corresponding to *Re*=100, departs by a maximum of 10%. Therefore the angle from the y-axis, intercepting the location x/w=3.67, at the wall, was taken to be φ_{max}. Hence:

$$\varphi_{max} = tan^{-1}\left(\frac{3.67}{5}\right) = 0.633\ rd = 36.28^o$$

Interestingly, this average value of x/w happens to be the exact same value at which all three curves intersect (those of *Re*=250, and 400, being almost overlapping for |x/w|<5), as shown in Fig. 2 above. This definition of φ_{max} was considered to be solid, since it was based on a feature that characterizes a fair span of the self-stable *Re* range, established by [5].

The finite volume CFD code FLUENT, was used to solve this problem. After a time and space grid independence study, and taking the convergence behavior along with the computational time into account, it was found that a structured 250x120 mesh was an adequate grid, with a time step of 0.1ms using a first order implicit transient formulation. The elements were refined near the walls to capture the high gradients.

The SIMPLE scheme was used for the pressure-velocity coupling, together with a second order upwind discretization scheme for the convective terms in the momentum and energy equations.

Convergence criteria were set to 10^{-6} scaled residuals for the continuity and momentum equations, and 10^{-8} scaled residuals for the energy equation.

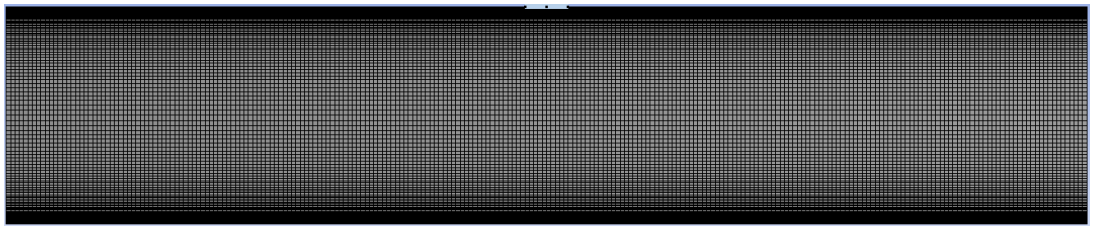

Fig. 3 – The mesh used to solve the current problem

3. VALIDATION PROBLEM

Before any simulation is carried out in the present study, and in order to be confident about the commercial CFD code being used, the case of *Re*=250 simulated by [5], was computed again using the ANSYS FLUENT commercial code.

The same spatial boundary conditions, as those of the current problem (also, matching those used by the original study of [5]), were used, with a constant downward velocity at the inlet. The same mesh shown in Fig. 3 above, along with the discretization and pressure-velocity coupling schemes mentioned above were used.

Since the study of [5] showed that a Reynolds number of 250 belongs to the self-stable range, it was safe to model the flow as steady. The data comparison is shown in Fig. 4 below.

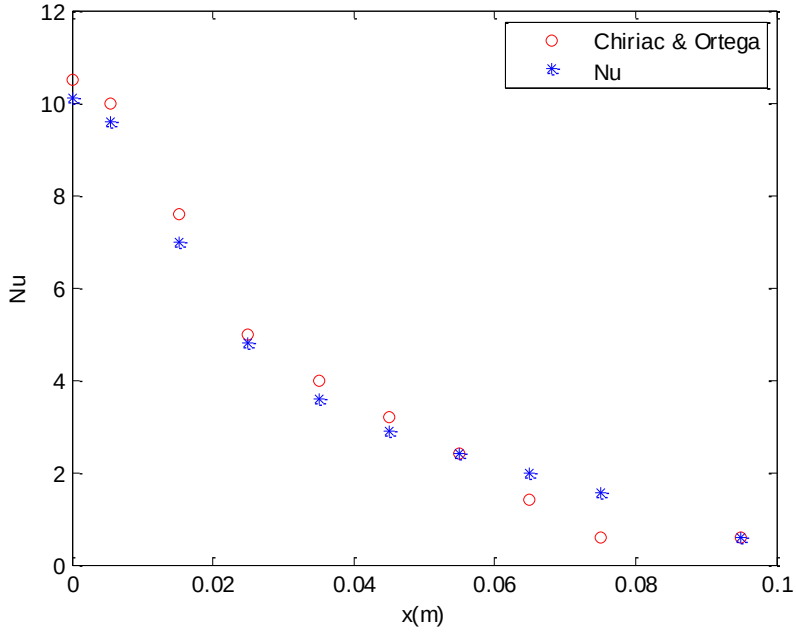

Fig. 4 – Comparison of the obtained *Nu* distribution to the one obtained by Chiriac and Ortega

Both data sets were symmetric about the y-axis, so only one side of the channel was taken for comparison.

The data almost perfectly agreed at x=0.055m, and 0.095m. Beside the different schemes used for the discretization of the convective terms in the energy and momentum equations ([5] used the QUICK scheme), the difference in the results is mainly due to the difference between the grids.

In contrast to the grid shown in Fig. 3, the grid used in the original study is an 84x62 grid, yet, the significantly refined 250x120 grid seemed necessary, since it gave the best convergence behavior for the currently treated problem.

As an overall assessment, the entanglement of the plots is smooth enough to make them compare well.

Having these results in hand, the way was clear for the simulations of the current problem to be carried out with confidence about the results to be obtained afterwards.

4. RESULTS AND DISCUSSIONS

Eight frequencies were studied, for *Re*=250, these are in dimensionless form: *St*=0.05, 0.1, 0.2, 0.3, 0.4, 0.5, 0.6, and 0.75; respectively corresponding to the following dimensional frequencies: 1Hz, 2Hz, 4Hz, 6Hz, 8Hz, 10Hz, 12Hz, and 15Hz.

The two lowest frequencies, *St*=0.05, and 0.1, exhibited flow fields that would be considered counter intuitive at the first glance; because of the significant asymmetry. Both flows were more developed to the right side of the channel as shown in the velocity contours of Fig. 5 below.

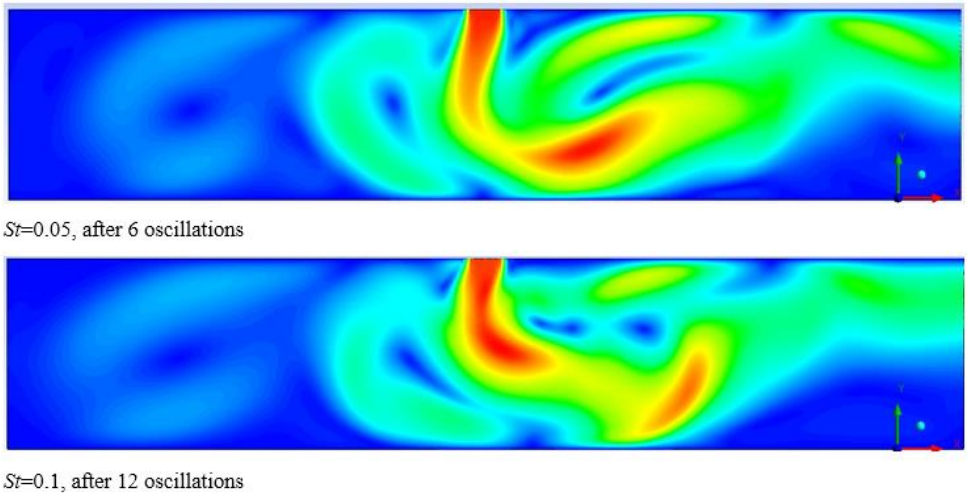

Fig. 5 – Snapshots of the velocity distributions for *St*=0.05, and 0.1

The cause underlying this behavior resides in the fact that the first swing of the jet is to the right. At such low frequencies, the duration of the first swing, is long enough for the flow to entrain the nearby fluid, to the right. This entrained fluid will have gotten far enough, to make it harder for the next swing that is to the left, to restore balance. Which breaks the symmetry, because the third swing, will be to the right side that already have a more developed flow. Hence, this imbalance will be amplified during every oscillation period; which explains the right side developed flow fields shown above. One might suspect the flow fields to eventually become symmetric if given enough time. But the reason why this is most probably not the case, is the persistence of this flow pattern even when the frequency is doubled; allowing only half the time for the first right swing to initiate a flow to a preferable side, and giving a double amount of left swings to compensate for the imbalance. This effect will eventually disappear, for greater values of *St* as demonstrated later.

Since heat transfer is a strong function of the flow field, one should expect a similar asymmetry for the *Nu* distribution over the wall as shown in Fig. 6 below. Nusselt distributions were obtained by averaging instantaneous distributions over the last 2 periods for *St*=0.05, and the last period for *St*=0.1.

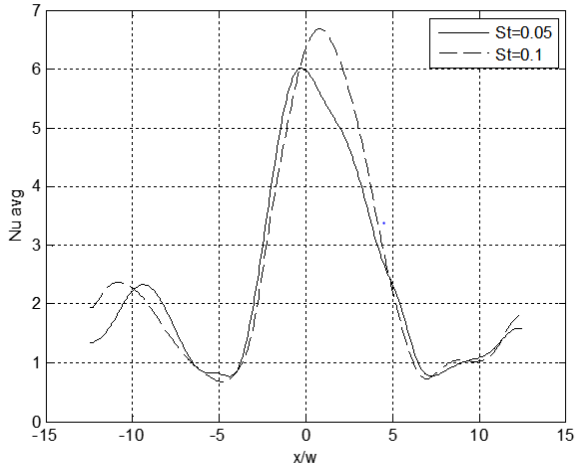

Fig. 6 – The average *Nu* distributions for *St*=0.05, and 0.1

One may notice a significant local peak near *x*/w=-10 for both frequencies. This is due to the vortices above that location as shown in Fig. 5, which agrees with the findings of [1].

Nusselt number data corresponding to *St*=0.05 and 0.1, were excluded from the comparison conducted in Fig. 7 and Fig. 8 since they presented extreme cases in which the flow is asymmetric, as discussed earlier. However, they were presented to illustrate the effect that led to asymmetric flow fields for greater values of *St*.

Due to the recirculation zones at about |x/w|=12, Nusselt was higher for the oscillating jet, than that of the steady jet. This was the case for all Strouhal numbers considered at 8<|*x*/w|<12.5 with a maximum enhancement of about 330%. On the other hand, at |*x*/w|=7.5, the steady jet had a 155% higher Nusselt number value than that corresponding to the oscillating jet. Looking at the temperature contours, one can see the inflated diffusive layer at |*x*/w|=7.5. This can be attributed to the reduced span-wise velocity as a part of the flow is forced to move between the central and the outer recirculating regions, in the case of an oscillating jet.

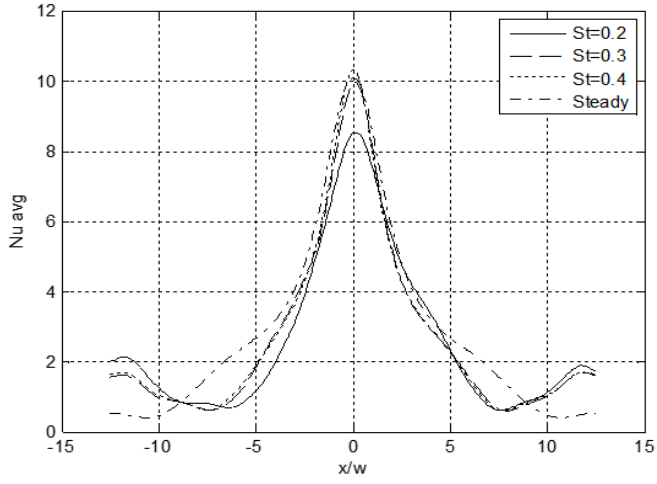

Fig. 7 – *Nu* comparison of the three lowest values of *St*, with the steady case for *Re*=250

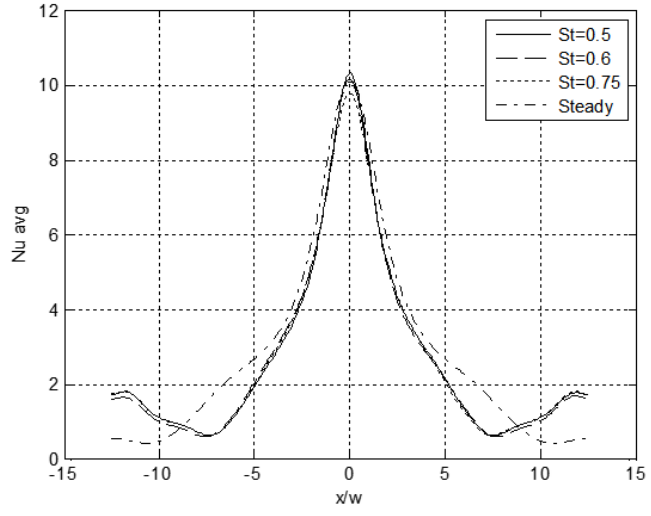

Fig. 8 – *Nu* comparison of the three highest values of *St*, with the steady case for *Re*=250

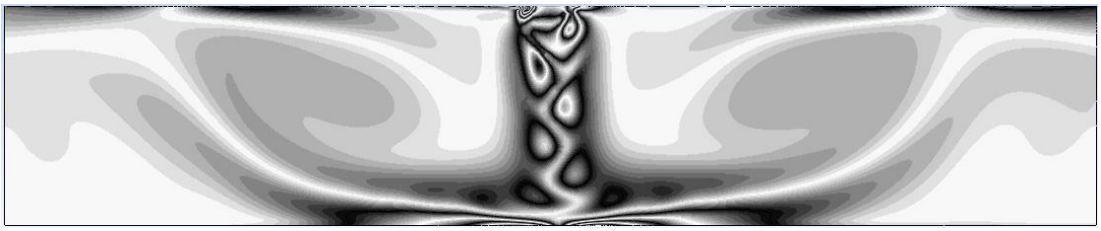

Fig. 9 – A snapshot of the vorticity contours at tf=48 (tf is the number of oscillations) for *Re*=250 at *St*=0.4

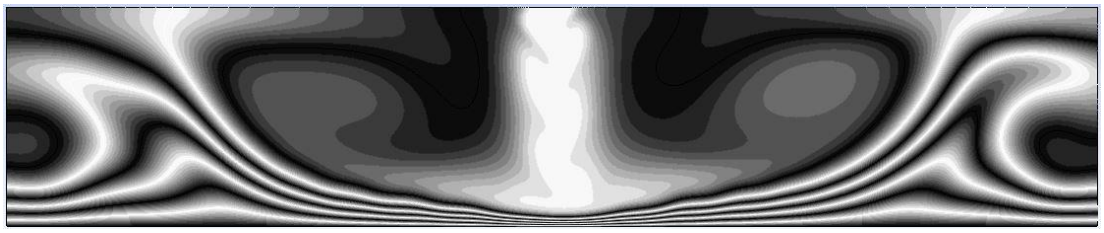

Fig. 10 – A snapshot of the temperature contours at tf=48 for *Re*=250 at *St*=0.4

Table 1 – Comparison of the Average Nu_0 for *Re*=250

St	$\boldsymbol{Nu_0}$
steady	10.09
0.2	8.54
0.3	9.96
0.4	10.31
0.5	10.30
0.6	10.15
0.75	9.77

From the tabulated results above, *St*=0.4 had the highest corresponding Nu_0 of 10.31, with the one corresponding to *St*=0.5 coming just after, with a value of 10.30; which presents an improvement over the value that the steady jet reached, by about 2.2 %.

For Re=100, five Strouhal numbers were studied, St=0.4, 0.45, 0.5, 0.625, and 0.75; corresponding to the following frequencies: f=3.2Hz, 3.6Hz, 4Hz, 5Hz, and 6Hz, respectively.

At this value of Re, the average Nu distribution showed no improvement over the steady jet case; regardless of the considered Strouhal number values.

As *St* was varied from 0.4 to 0.625, the *Nu* distribution did not change substantially. At *St*=0.75, Nusselt number was significantly decreased in the stagnation region.

A comparison of the time averaged Nusselt number distributions, for the different frequencies considered for *Re=100*, is shown in Fig. 11 and Fig. 12 below.

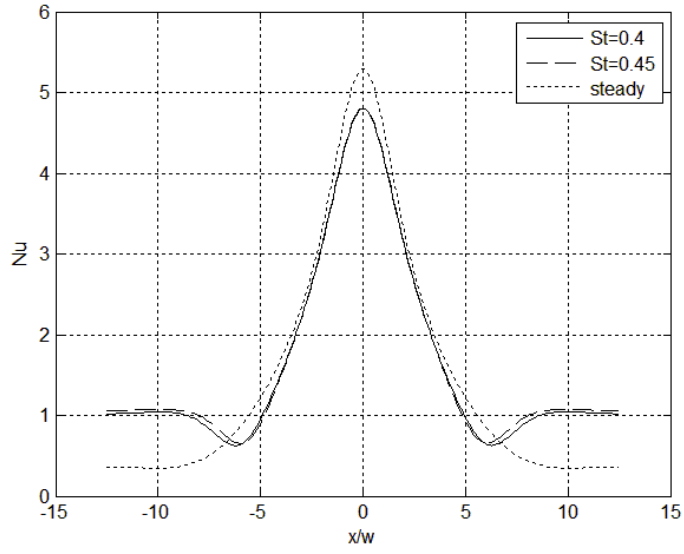

Fig. 11 – *Nu* comparison of the two lowest values of *St*, with the steady case

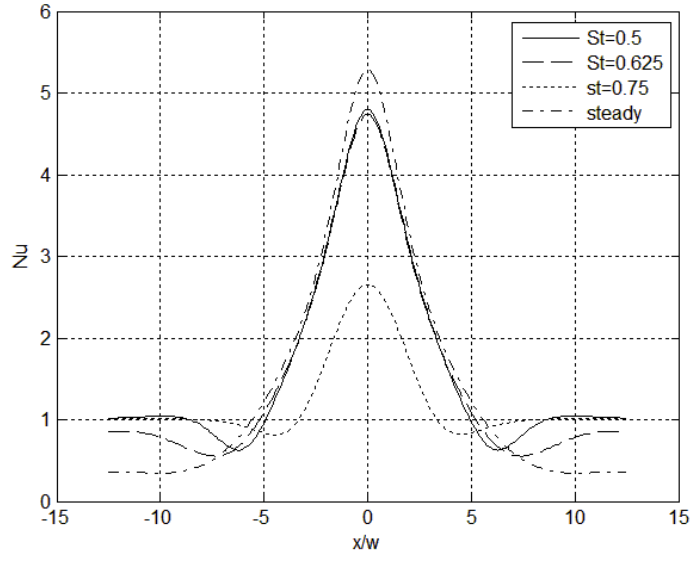

Fig. 12 – *Nu* comparison of the three highest values of *St*, with the steady case

Table 2 – Comparison of the Average Nu_0 for *Re*=100

St	Nu_0
steady	5.29
0.4	4.8
0.45	4.81
0.5	4.79
0.625	4.74
0.75	2.65

Compared to its 1.25% decrease from *St*=0.4 to *St*=0.625, Nu_0 suddenly decreased by 44.1% when *St* increased from 0.625 to 0.75, a fact that was attributed to the severe oscillation that led to a drastically decayed bulk momentum, with no vortices to compensate for this effect.

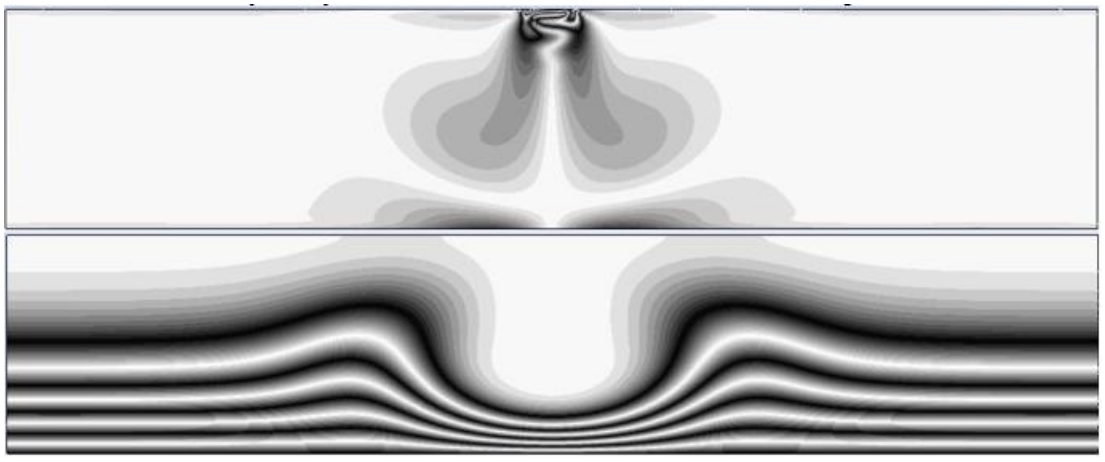

Fig. 13 – A snapshot of the vorticity (upper) and temperature (lower) contours at tf=36 for *Re*=100 at *St*=0.75

As pointed out in the introduction, the main objective of this study is to engage the jet into flapping, when Reynolds number is in the self-stable range, presented by the study of Chiriac et al. [5]. At *Re*=400, flapping could be triggered by the inlet's oscillating conditions. Three frequencies were considered for this *Re* value. These are: *St*=0.4, 0.5, and 0.75, corresponding to 12.8Hz, 16Hz, and 24Hz, respectively. The case of *St*=0.5 was simulated for 2 additional seconds, where it turned out that, a few periods after flapping was established, the jet permanently leaned to the left. However, at St=0.75 flapping was more stable and lead to a better heat transfer at the stagnation.

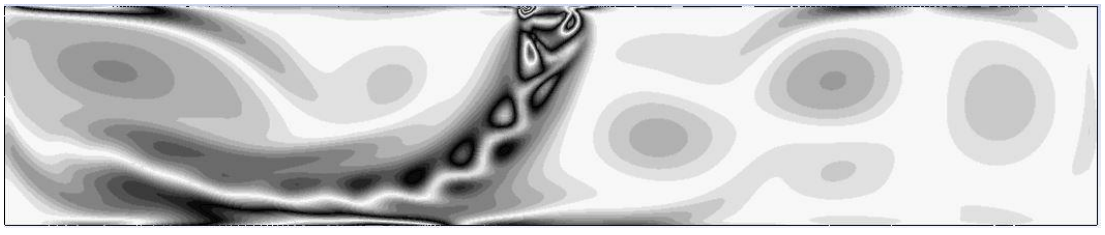

Fig. 14 – Instantaneous vorticity contours at tf=132 for *Re*=400 at *St*=0.5

One possible explanation of the mechanism underlying this behavior is as follows. Due to the initial condition effect explained in the beginning of the chapter, the flow will initially have a higher momentum in the right wall jet region, and hence, will be less prone to separation. In the meantime, the lower momentum fluid in the left wall jet region, will separate earlier, and therefore, at a closer distance to the jet. Then the re-entrainment effect caused by the jet will take over the left separated flow, which will cause the latter to build up a strong recirculation that is close to the jet. This recirculation will eventually drag the jet to the left, as the farther right recirculation weakens.

In the figure shown below, it is obvious that the diffusive layer got thicker, yielding the significantly lower Nu. This is due to the entrained heated fluid coming from the right side of the channel.

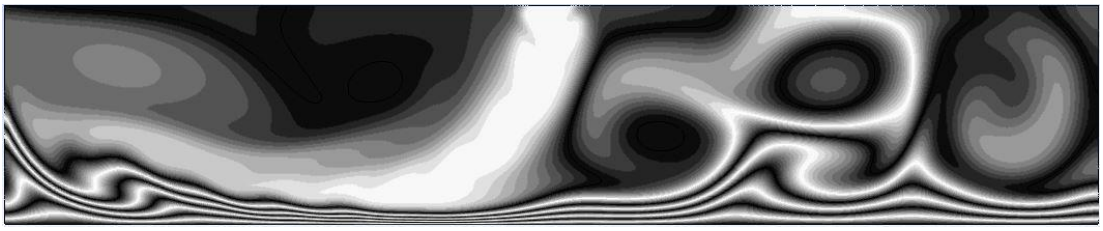

Fig. 15 – Instantaneous temperature contours at tf=132 for *Re*=400 at *St*=0.5

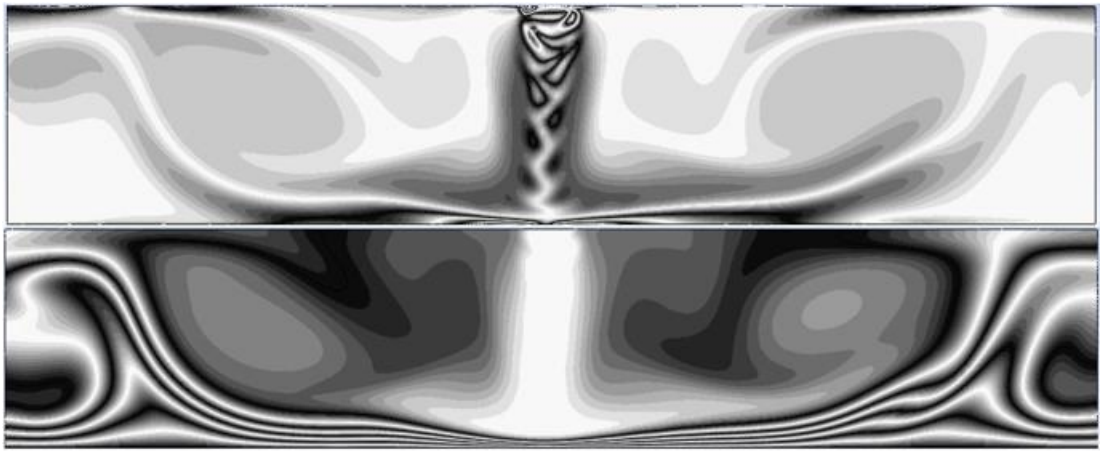

Fig. 16 – Instantaneous vorticity(upper) and temperature(lower) contours at tf=120 for *Re*=400 at *St*=0.75

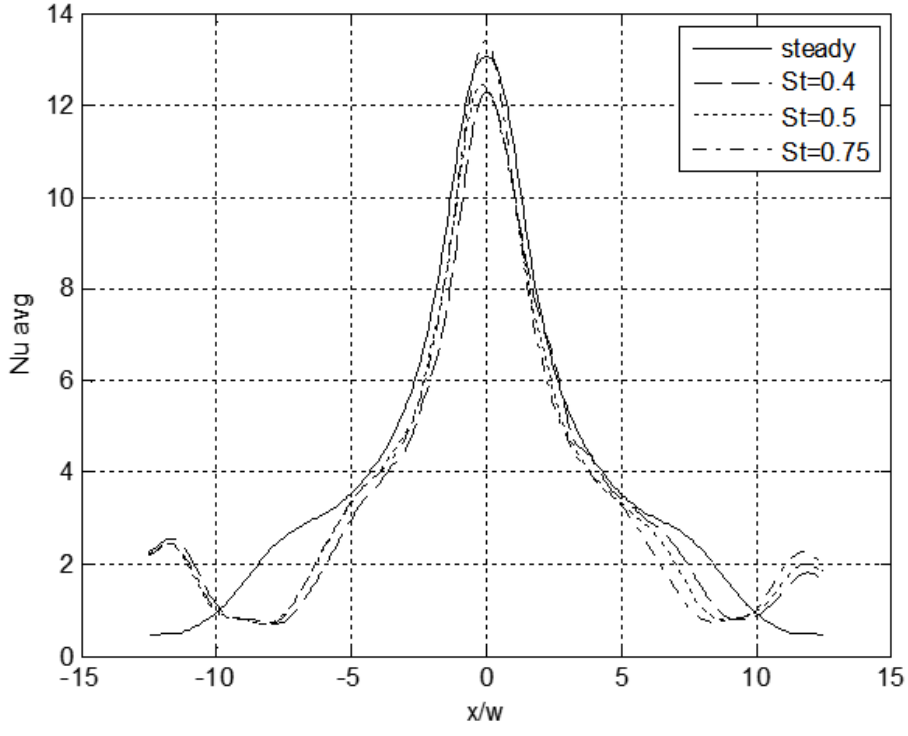

Fig. 17 – Comparison of *Nu* distributions for *Re*=400

Table 3 – Comparison of the Average Nu_0 for Re=400

St	Nu_0
Steady	13.06
0.4	12.29
0.5	12.45
0.75	13.38

From the comparison table shown above, the average Nu_0 corresponding to St=0.75 had a dim 2.45% improvement over that of the steady jet.

REFERENCES

[1] M. Ebrahim, L. Silva and A. Ortega, *Heat transfer due to the impingement of an axisymmetric synthetic jet emanating from a circular orifice: A numerical investigation of a canonical geometry*, Proceedings of the International Technical Conference and Exhibition on Packaging and Integration of Electronic and Photonic Microsystems (InterPACK2013), 2013, Burlingame, California, USA.

[2] S. Marzouk, H. Mhiri, S. El Golli, G. Le Palec and P. Bournot, Numerical study of momentum and heat transfer in a pulsed plane laminar jet, *International Journal of Heat and Mass Transfer*, vol. **46**, pp. 4319-4334, 2003.

[3] P. Hee Joo, K. Kurichi and S.M Arun, Heat transfer from a pulsed laminar impinging jet, *International Communication of Heat and Mass Transfer*, vol. **32**, pp. 1317-1324, 2008.

[4] D. Kim, A Numerical study on heat transfer in laminar pulsed slot jets impinging on a surface, *World Academy of Science, Engineering and Technology*, **6**, 2012-09-20.

[5] V. A. Chiriac and A. Ortega, A numerical study of the unsteady flow and heat transfer in a transitional confined slot jet impinging on an isothermal surface, *International Journal of Heat and Mass Transfer*, vol. **45**, pp. 1237-1248, 2002.

[6] C. Camci and F. Herr, Forced convection heat transfer enhancement using a self-oscillating impinging planar jet, *Journal of Heat Transfer*, vol. **124**, no. 4, DOI: 10.1115/1.1471521, 2002.